(2)

UV Photochemistry of Trivinylantimony Adsorbed on Quartz

J. A. Tarr, S.-P. Lee, and M. C. Lin

Department of Chemistry

Emory University

Atlanta, GA 30322

N00014-89-J-1235

1991

Abstract

The surface photochemistry of trivinylantimony adsorbed on a cold quartz surface was investigated using pulsed 193 nm excimer- laser radiation. The major desorption products observed were C_2H_2, C_2H_3, C_2H_4, C_4H_6, Sb, $Sb(C_2H_3)$, $Sb(C_2H_3)_2$, $Sb(C_2H_3)_3$ and Sb_2. Photoproduct distributions and their Maxwell-Boltzmann characteristic temperatures were determined using time-of-flight mass spectrometry, incorporating both electron impact and, for Sb detection, resonance-enhanced multiphoton ionization. Photoproduct yields and Maxwell-Boltzmann temperatures were dependent on photon fluence, sample dosage, and surface temperature. The Maxwell-Boltzmann temperatures of the C_xH_y products were substantially lower than those of the metallic and organometallic species, indicating that the desorption of the Sb-containing products probably occur via electronically excited states. A mechanism is given for the photochemistry of adsorbed trivinylantimony.

1. Introduction

Antimonides have played an important role in mixed semiconductor materials [1,2]. Trivinylantimony (TVSb) is a promising source for organometallic chemical vapor deposition (OMCVD) of III/V semiconductors containing antimony. The gas-phase thermal decomposition of TVSb as a source for organometallic vapor-phase epitaxy has recently been investigated [3]. This compound may also serve as a laser chemical vapor deposition (LCVD) source.

The mechanism of the photodecomposition of TVSb is not known. It is important to understand the mechanism of TVSb photolysis in order to fully utilize it as a source of Sb in LCVD processes. In this initial investigation, TVSb adsorbed on quartz at low temperatures was photolyzed with excimer laser radiation and the desorbed photoproducts analyzed by time-of-flight mass spectrometry to determine the mechanism.

2. Experimental

The experimental apparatus is similar to the one employed in our previous study of dimethylgold hexaflourocetylacetonate photodecomposition reaction [4]. The schematic diagram of the apparatus is given in fig. 1. It consists of two differentially-pumped chambers; a sample chamber with an Edwards model 160 Diffstak diffusion pump, and a detection chamber with a Leybold turbomolecular pump. The quartz substrate in the sample chamber is aligned so that species desorbing from the surface are collected through a 3 mm skimmer between the chambers and are directed into the ionization region of the detection chamber.

The SiO_2 (UV grade fused silica) surface was mounted in a brass sample holder attached to a liquid nitrogen reservoir, allowing the sample holder to be cooled

to 145 K. A heater was also attached to the surface holder allowing controlled temperatures for temperature-dependent studies.

The liquid TVSb sample was maintained at ice temperature, with a vapor pressure of 1.26 Torr. The sample was dosed from an inlet manifold through a stainless steel capillary tube onto the quartz surface. For most of the experiments, the chamber pressure and laser repetition rate were 5x10-7 Torr and 10 Hz, giving a dosage of < 0.1 Langmuir (10^{-6} Torr.sec).

The ultraviolet absorbance spectrum of TVSb was measured with a Cary 1/3 spectrophotometer. The vapor was measured in the pressure range of 0.135 to 5.185 Torr in a 12.5 cm sealed cell. The slit band width was 1.0 nm. The extinction coefficient at 193 nm was determined to be 16687 L/mol.cm.

The surface photochemistry was studied by using a Lambda Physik EMG-102 laser operating with Ar fluoride to obtain the 193 nm radiation. The laser energy was variable from a few mJ/pulse to 8.5 mJ/pulse. The beam was guided onto the surface to produce a rectangular beam approximately 1 cm^2 across the diameter of the surface.

The detection of desorbed photoproducts was done with an Extrel Quadrupole Mass Spectrometer. Ionization of products entering the QMS was achieved by electron impact ionization. Selective photo-ionization by REMPI (resonance enhanced multiphoton ionization) was achieved with a Lambda Physik EMG 201 and FL3002 excimer-pumped dye laser system. The ion signals were collected with a channeltron ion multiplier, amplified and then recorded with a Nicolet 450 digital waveform acquisition system. REMPI signals were recorded through a Stanford Research model 250 and 245 gated boxcar integrator system and an IBM-PC/AT computer. Lasers and detection systems were controlled by a Stanford Research model DG535 digital pulse generator.

3. Results

An overall view of the 193 nm photofragmentation patterns of adsorbed TVSb is shown in fig. 2 in terms of their time of flight (TOF) profiles. The C_xH_y products show a significant difference in flight time from the antimony containing species. The fragment TOF profiles could be deconvoluted into photodissociation (PDIS) and photodesorption (PDES) components. The latter component refers to the desorption of TVSb, whose ions fragment to give smaller ions in the ionizer of the mass spectrometer.

The TOF profiles of the C_2H_n photoproducts indicate that these species originate from photolysis of TVSb at the surface. These TOF-profiles can be characterized by various Maxwell-Boltzmann temperatures (T_{MB}). The values of the T_{MB}'s of the important species are presented in table 1. The fragment T_{MB}'s are reported for the deconvoluted component corresponding to the species formed from PDIS at the surface. The relative contributions from PDIS and PDES are also given.

The relative photofragment yields are compared in fig. 3, which shows the total ion count of each species, normalized to the parent TVSb (m/z = 202). Gas phase $TVSb^+$ fragmentation pattern is also shown for comparison. There is a significant differnce between the parent ion signals and those of the desorbed photofragments, suggesting a high degree of photofragmentation at the surface.

3.1 Dosage Dependence

The dependence of the desorption yield of TVSb on surface coverage was examined by changing the laser repetition rate while maintaining a constant sample pressure. The rate was varied from 0.1 to 20 Hz with a chamber pressure of $5x10^{-7}$ Torr.

The dosage dependence of the TOF profile of the desorbed TVSb is shown in fig. 4. Both T_{MB} and desorption yield increased with coverage of less than 0.1 L, as

expected from PDES [5]. Above this coverage, large deviations from linearity were observed. All other experiments were performed at coverages of ≤0.1 L per pulse.

The effects of surface coverage on T_{MB} and the angular dependence of desorption yields have been studied in detail by Polanyi and coworkers [6,7]. For example, the desorption of OCS from LiF(100) was found to have a sharp variation in the angular distribution from cos θ with ~0.001L exposure to $\cos^{11}\theta$ with 21L exposure [8]. The enhancement of the desorption yield toward surface normal at higher coverages is believed to result from the reduction in the sideway motion and thus the permitted cone-of-escape angles. This also leads to significant momemtum transfer which results in higher T_{MB}'s at higher coverages.

3.2 Laser Fluence Dependence

The dependence of the parent photodesorption yield on laser fluence is given in fig. 5. Increasing the laser fluence produces an increase in T_{MB} which levels off with higher fluences. Figure 6 shows the desorption yields of the products, normalized to the parent yield. The desorption yield increases with fluence rising sharply at higher fluence. This effect is more pronounced with C_2H_2, C_2H_3, and $Sb(C_2H_3)$ than with the other products. The C_2H_4 relative yield decreases at the highest fluences, while C_4H_6 and the other C_xH_y species yields increase. These products were formed at the expense of C_2H_4. The increase in the yields of these products at higher fluences may in part be due to a multiphoton excitation effect.

3.3 Temperature Dependence

The substrate temperature was varied from 147 to 165 K by heating the brass sample holder while it was in contact with the liquid N_2 reservoir. Increasing the temperature caused a decrease in both photodesorption yield and T_{MB}. This result is fully consistent with the coverage dependence discussed in the preceding section

since coverage decreases with increasing temperature when the dosage remains constant.

3.4 Desorption Products

The desorbed neutral species detected by EI/MS were C_2H_2, C_2H_3, C_2H_4, C_4H_6, Sb, $Sb(C_2H_3)_n$ (n=1,2 and 3), and Sb_2. Atomic hydrogen was detected by EI/MS and TOF profiles were obtained. Since H can originate from all of the other species detected, a clear picture of its T_{MB} could not be determined. At higher laser fluences, ions were also detected with much higher translational energies than the neutral species. An ion reflector was employed to remove ions before they reached the mass spectrometer.

3.4.1 Sb-Containing Products

The TOF profiles of the organometallic species show multiple components. There is one component due to the cracking of the parent TVSb in the EI region and another faster component. This indicates that these products were formed to a large extent through PDIS and originated from the surface. As with the C_xH_y products, the PDIS channel becomes more prominent with higher laser fluences.

The deconvolution of the $Sb(C_2H_3)_n$ ($n \leq 3$) fragments can be carried out in a relatively straightforward manner. As illustrated in fig. 3, the divinylantimony (DVSb) ion fragment derived from both the cracking of the parent TVSb (n=3) ion and from surface photolysis is small. We therefore expect that the monovinyl antimony (MVSb) and antimony ion-signals originate mainly from the individual photolysis products and from the fragmentation of the parent $TVSb^+$ ion in the ionizer. Since the TOF-profile of $TVSb^+$ is well charaterized without other interferences, both DVSb and MVSb TOF-profiles can be reliably deconvoluted. The deconvoluted $Sb(C_2H_3)_n$ TOF-profiles

indicate that these photo-products desorb from the surface with much higher translational energies than their hydrocarbon counterparts (see Table 1).

The deconvolution of the Sb signal obtained by EI/MS can be achieved in a similar manner as illustrated in fig. 7 B. The figure shows the faster Sb^+ component deriving from the neutral Sb product and the slower components formed mainly from the fragmentation of $TVSb^+$ and $MVSb^+$ in the ionizer. The deconvoluted fast TOF component agrees well with the one obtained by the laser ionization (REMPI/MS) as shown in fig. 7A. The small deviation appears in the figure between the deconvoluted Sb^+ EI-signal and the Sb^+ REMPI signal at longer flight times may arise from Sb_2^+ generated by the REMPI of Sb_2. This possibility will be examined in the future.

The REMPI spectrum of Sb is given in the inset of fig. 7A. Table 2 summarizes all detected transitions in this wavelength region. All major peaks have been identified [9]; the key ones are labeled with the responsible transition given in the figure caption. The REMPI/TOF profile was measured by changing the delay between the photolysis and the REMPI laser, which was set at 269.18 nm. The REMPI spectrum presented in the inset of fig. 7A was measured at the peak of the TOF profile by scanning the wavelength.

The TOF profile of Sb_2 is shown in the inset of fig. 2. Diantimony is not observed in the gas phase mass spectrum of TVSb and must originate from the surface by the recombination-desorption process: Sb(a) + Sb (a) $\rightarrow$ Sb_2 (a) $\rightarrow$ Sb_2 (g). The TOF profile given in fig. 2 could be well characterized by a Boltzmann temperature T_{MB} = 1852 K under the conditions specified in Table 1.

3.4.2 Hydrocarbon Products

The H, C_2H_2, and C_2H_3 species were found to be ejected directly from the surface and their ions were also formed in the EI region from the cracking of larger molecules. This is determined from the TOF profiles which indicated contributions from

both photodesorption (PDES) and photodissociation (PDIS) channels. At higher fluences, the PDIS/PDES ratio increases due to stronger absorption and the increasing probability of two-photon absorption. There is also a smaller, much slower component attributed to some other desorption process. One such possibility is the slow diffusion/desorption of photofragments into the line-of-sight of the QMS detector. The C_2H_4 and C_4H_6 products also have TOF distributions showing multiple components, originating from photoreaction at the surface and from the fragmentation of $TVSb^+$ in the mass spectrometer, similar to the Sb-containing species as discussed above.

4. Discussion

The photolysis of TVSb adsorbed on a quartz surface by 193 nm radiation leads to both PDIS and PDES. The observed PDIS species are C_2H_2, C_2H_3, Sb, $Sb(C_2H_3)$, and $Sb(C_2H_3)_2$. Ethene, 1,3-butadiene, and diantimony were also produced, probably via combination reactions at the surface, followed by desorption:

$$C_2H_3\ (a) + H\ (a) \rightarrow C_2H_4\ (a) \rightarrow C_2H_4\ (g)$$

$$C_2H_3\ (a) + C_2H_3\ (a) \rightarrow C_4H_6\ (a) \rightarrow C_4H_6\ (g)$$

$$Sb\ (a) + Sb\ (a) \rightarrow Sb_2\ (a) \rightarrow Sb_2\ (g)$$

1,3-Butadiene may also form by direct elimination [3]:

$$(C_2H_3)_3Sb\ (a) + h\upsilon \rightarrow (C_2H_3)Sb\ (a) + C_4H_6\ (g)$$

although it is believed to be less important mechanistically. On the basis of the known absorption spectrum of TVSb, there is an electronic state which is accessible by 193 nm UV absorption. This absorption leads to a high yield of photofragmentation.

The relative yields of PDIS and PDES and the T_{MB}'s of the observed products are dependent on surface coverage, surface temperature, and laser fluence. The metal-containing products desorb with much higher T_{MB}'s than C_2H_n products do.

This observation strongly suggests that the metallic species [Sb, Sb_2, $Sb(C_2H_3)_n$] can be easily electronically excited by the 193 nm radiation on the surface. The electronic energies, upon relaxation, can be effectively utilized for desorption.

Figure 3 shows that both desorption yield and T_{MB} of TVSb are affected by the amount of surface exposure. These results, at coverages less than 0.1 L, are similar to those found by others[6,7,8]. At higher coverages the dependence deviates from linearity because the desorption of TVSb becomes photon-limited.

The density of laser radiation incident on the surface affects the T_{MB}'s and yields of photoproducts. This is seen in figures 5 and 6. The data show an increasing effect on yield, and at the highest fluence, a large jump in the yields of photofragments was observed. This is indicative of two-photon absorption.

4.1 Mechanism

The mechanism of the observed photoprocesses is presented below:

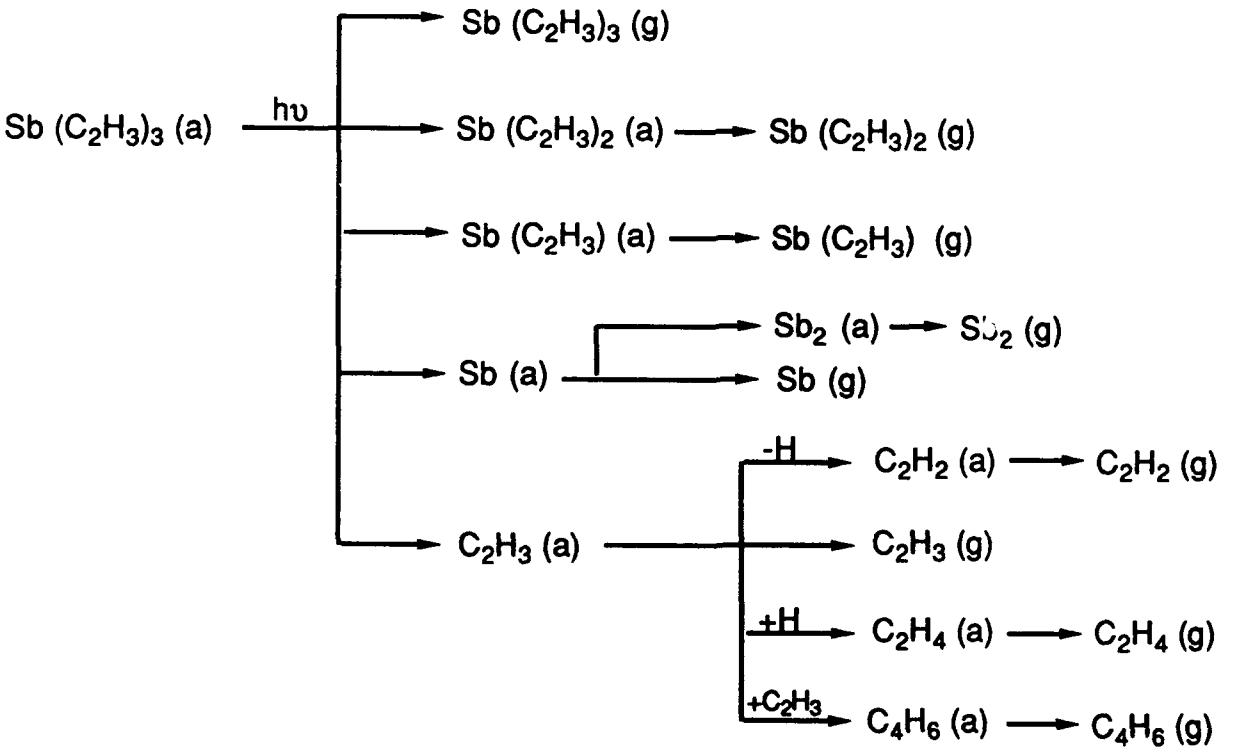

The mechanism differs greatly from that of the gas phase thermal decomposition process proposed by Larsen, et al.[3], wherein the major product formed is 1,3-butadiene. The fragmentation pathways give a high yield of products at the wavelength employed in this study.

The observed fragments, to a large extent, were produced from the surface through PDIS. The recombination products are formed as described above. Since the translational energies of the photoproducts are much smaller than those of the desorbed parent, the PDIS product desorption is clearly surface-mediated.

5. Conclusions

The surface photochemistry of TVSb adsorbed on a cold quartz surface has been determined to produce photoproducts of distributions which are very different than those decomposition products formed in the gas phase. The major difference is the formation of a high yield of C_2H_2, C_2H_3, and C_2H_4.

All of the photoproduct yields and characteristic temperatures were determined to be dependent on surface coverage, surface temperature, and laser fluence. The C_xH_y products formed through PDIS show T_{MB}'s which are much smaller than those of the organometallic species. This indicates that the Sb-containing species desorb by electronic excitation.

Acknowledgment

The authors gratefully acknowledge the support of this work by the Office of Naval Research.

References

[1]. Proceeding (Trudy) of the P.N. Lebedev Phys. Institute. Vol. 89 63-118. N. G. Basov, Ed. 1978.

[2]. H. Jorke, E. Kasper, H. Kibbel, H. Pristing, J. Appl. Phys. 68 (11) 1990.

[3]. C. A. Larsen, R. W. Gedndge, Jr., and G. B. Stringfellow, Chem. Mater. 3 (1991) 96.

[4]. J. A. Dagata, E. Villa, M. C. Lin, Appl. Phys. B. 51 (1990) 443.

[5]. I. Harrison, J. C. Polanyi, P. A. Young, J. Chem. Phys. 89 (3) (1988) 1475.

[6]. E. B. D. Bourdon, P. Das, I. Harrison, J. C. Polanyi, J. Segner, C. D. Stanners, R. J. Williams, P. A. Young, Faraday Discuss. Chem. Soc. 82 (1986) 343.

[7]. St. J. Dixon-Warren, K. Leggett, M. S. Matyjaszcyk, J. C. Polanyi, P. A. Young, J. Chem. Phys. 93(5) (1990) 3659.

[8]. J. C. Polanyi, P. A. Young, J. Chem. Phys. 93(5) (1990) 3673.

[9]. C. E. Moore, Atomic Energy Levels, vol III, NSRDS-NBS 35, National Bureau of Standards, 1971.

Table 1. Photoproduct T_{MB}'s and the relative contributions from the parent molecule, the fragment T_{MB}'s are reported for the deconvoluted TOF results.*

Observed ion (m/z+)	26	27	28	54	121	148	175	202	242
T_{MB}	972	957	816	875	1755	1534	2231	1066	1852
Relative Contribution									
C_2H_2	0.78								
C_2H_3		0.65							
C_2H_4			0.62						
C_4H_6				0.52					
Sb					0.09				
Sb (C_2H_3)					.43	0.26			
Sb (C_2H_3)$_2$							0.20		
Sb (C_2H_3)$_3$	0.22	0.35	0.38	0.48	0.48	0.74	0.80	1.00	
Sb_2									1.00

* Dosage = 0.1L, Fluence = 8.8 mJ/cm^2.pulse

Table 2. Observed Sb Transitions by (1+1) photoionization.[a]

Resonance Transition	λ_{obs} /nm	υ_{obs} /cm^{-1}	υ_{ref}[b] /cm^{-1}
6s $^2P_{3/2}$ ← 5p^2 $^2P_{1/2}$	269.26	37139	37133
6s' $^2D_{5/2}$ ← 5p^2 $^2P_{3/2}$	268.30	37272	37263
6s $^4P_{3/2}$ ← 5p^2 $^2P_{3/2}$	267.09	37441	37433
6s' $^2D_{3/2}$ ← 5p^2 $^2P_{3/2}$	265.30	37693	37687
6s' $^2D_{3/2}$ ← 5p^2 $^2P_{3/2}$	261.28	38273	38269
6s $^2P_{1/2}$ ← 5p^2 $^2D_{3/2}$	259.84	38486	38479
6s' $^2D_{3/2}$ ← 5p^2 $^2P_{1/2}$	257.44	38844	38837
6s $^2P_{3/2}$ ← 5p^2 $^2D_{5/2}$	252.90	39542	39537

(a). Both wavelength and frequency have been corrected for vacuum.

(b). Ref. [9].

Figure Captions

Figure 1. A schematic diagram of the experimental apparatus.

Figure 2. Photofragmentation pattern of adsorbed TVSb using 193 nm radiation. Laser fluence was 8.8 mJ/pulse. Dosage = 0.1 L, Inset: Comparison of TOF profiles of C_4H_6, Sb_2, and TVSb.

Figure 3. Comparison of relative mass spectrometric ion fragment yields for the desorbed surface photo-products from TVSb photolysis at 193 nm and the gas phase $TVSb^+$ ion fragmentation pattern. The intensities have been normalized to the parent ion.

Figure 4. Dependence of TVSb desorption yield on dosage with 193 nm irradiation. Fluence = 8.4 mJ/pulse.

Figure 5. Dependence of TVSb desorption on laser fluence with 193 nm irradiation. Dosage = 0.1L.

Figure 6. Dependence of product yields, normalized to the desorbed parent yield, on laser fluence.

Figure 7. A) REMPI/TOF profile of Sb. B) EI/TOF profile of Sb showing contribution from Sb and $Sb(C_2H_3)_3$. Inset: REMPI absorption spectrum of Sb from 250 - 275 nm. The labeled transitions are (i) $6s^2P_{3/2} \leftarrow 5p^2\ ^2D_{5/2}$, (ii) $6s^2P_{1/2} \leftarrow 5p^2\ ^2P_{1/2}$, (iii) $6s'\ ^2D_{3/2} \leftarrow 5p^2\ ^2P_{3/2}$, (iv) $6s\ ^2P_{3/2} \leftarrow 5p^2\ ^2P_{1/2}$.

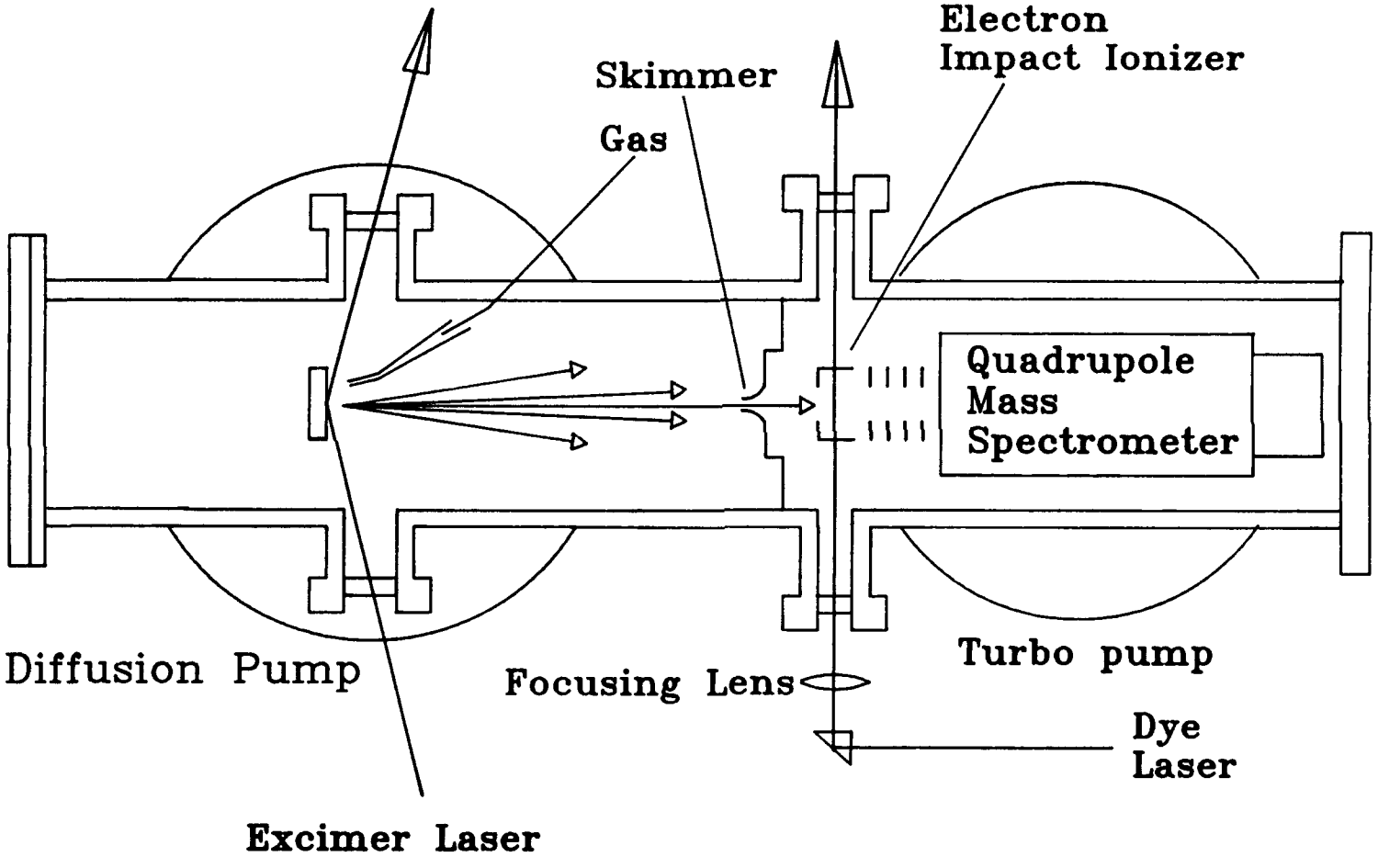
Electron
Impact Ionizer
Skimmer
Gas
Quadrupole
Mass
Spectrometer
Diffusion Pump
Focusing Lens
Turbo pump
Dye
Laser
Excimer Laser

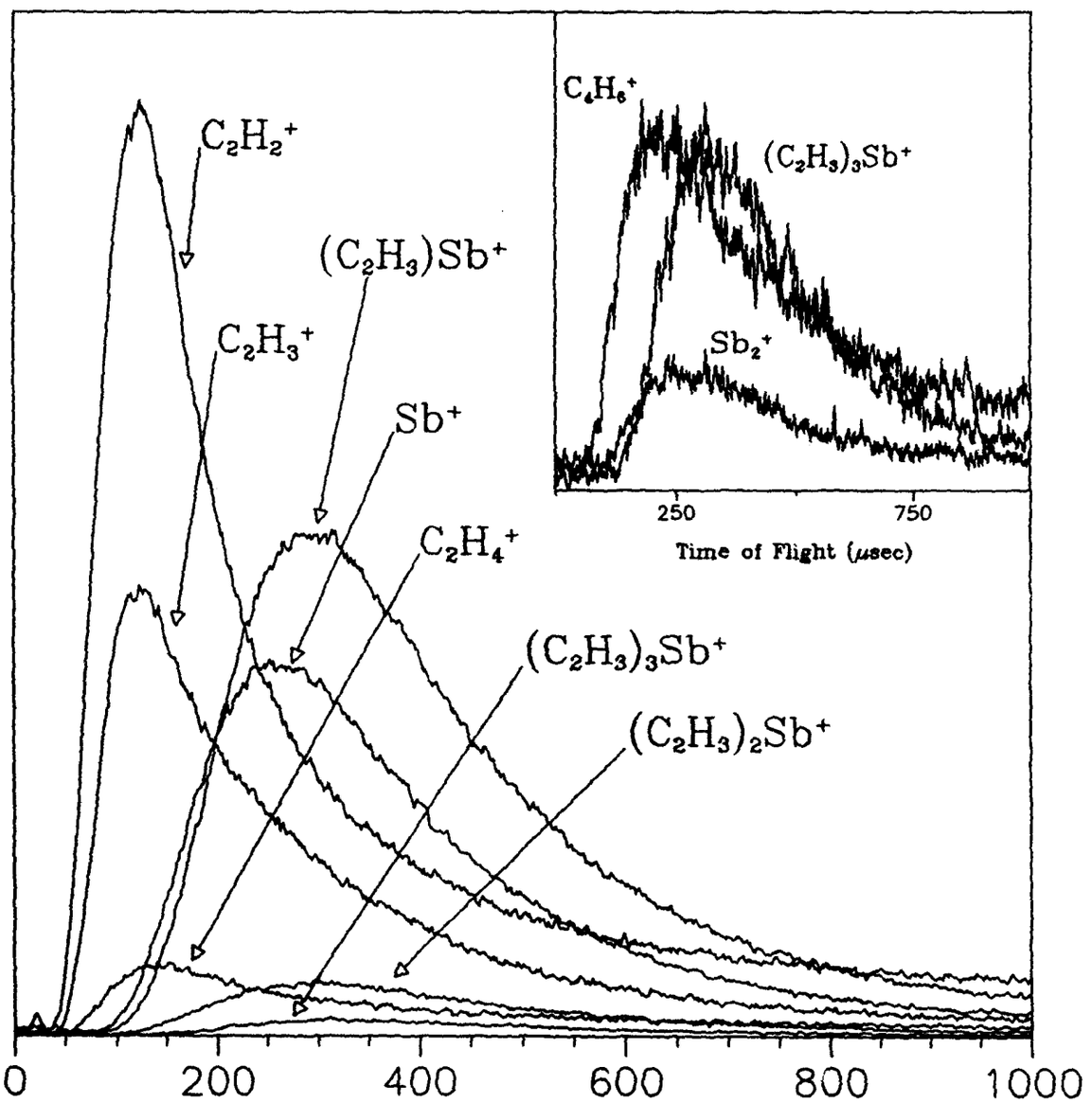
$C_2H_2^+$
$(C_2H_3)Sb^+$
$C_2H_3^+$
Sb^+
$C_2H_4^+$
$(C_2H_3)_3Sb^+$
$(C_2H_3)_2Sb^+$
$C_4H_6^+$
$(C_2H_3)_3Sb^+$
Sb_2^+
250
750
Time of Flight (μsec)
0
200
400
600
800
1000
Time of Flight (μsec)

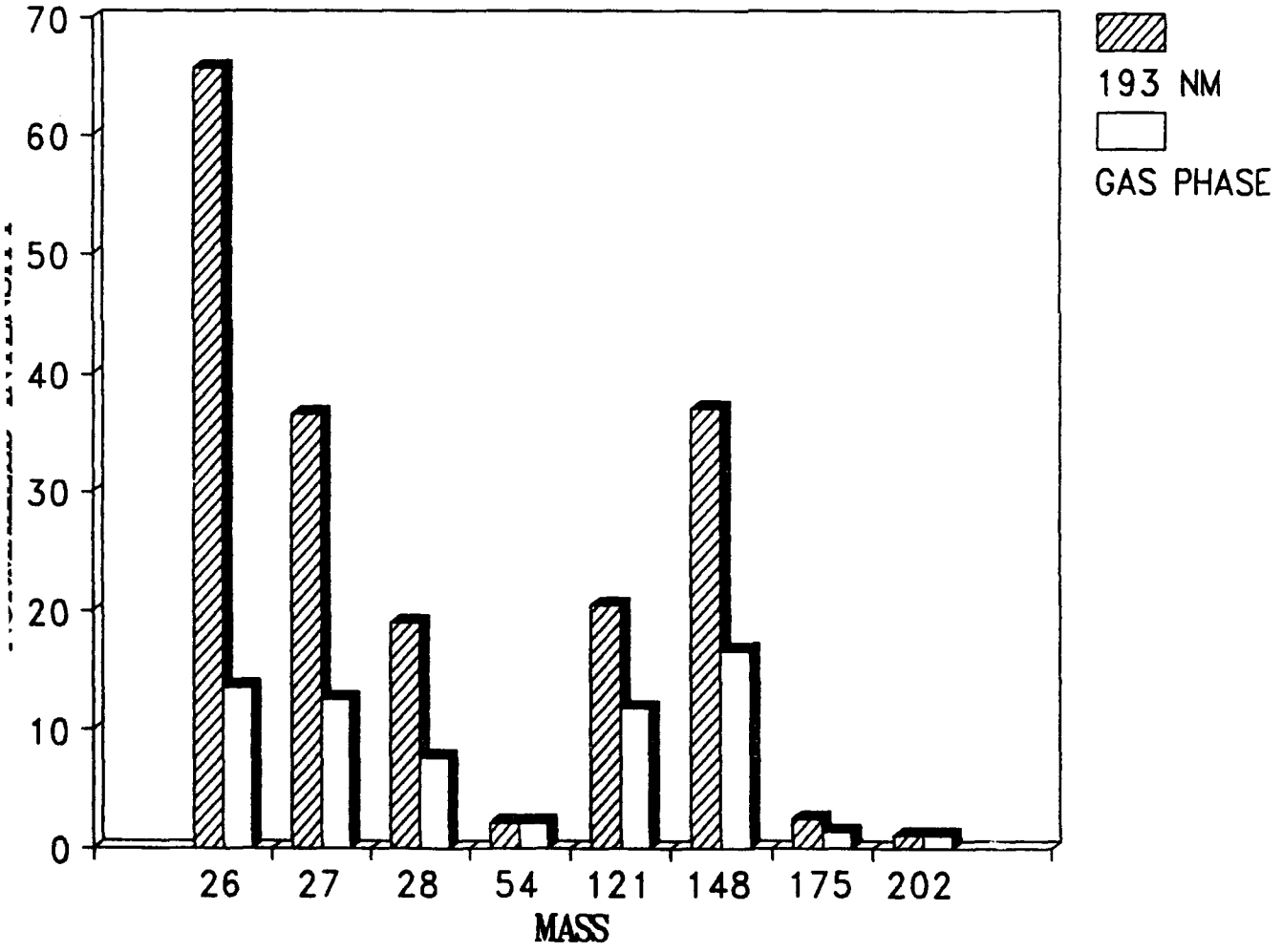
70
60
50
40
30
20
10
0
26
27
28
54
121
148
175
202
MASS
193 NM
GAS PHASE

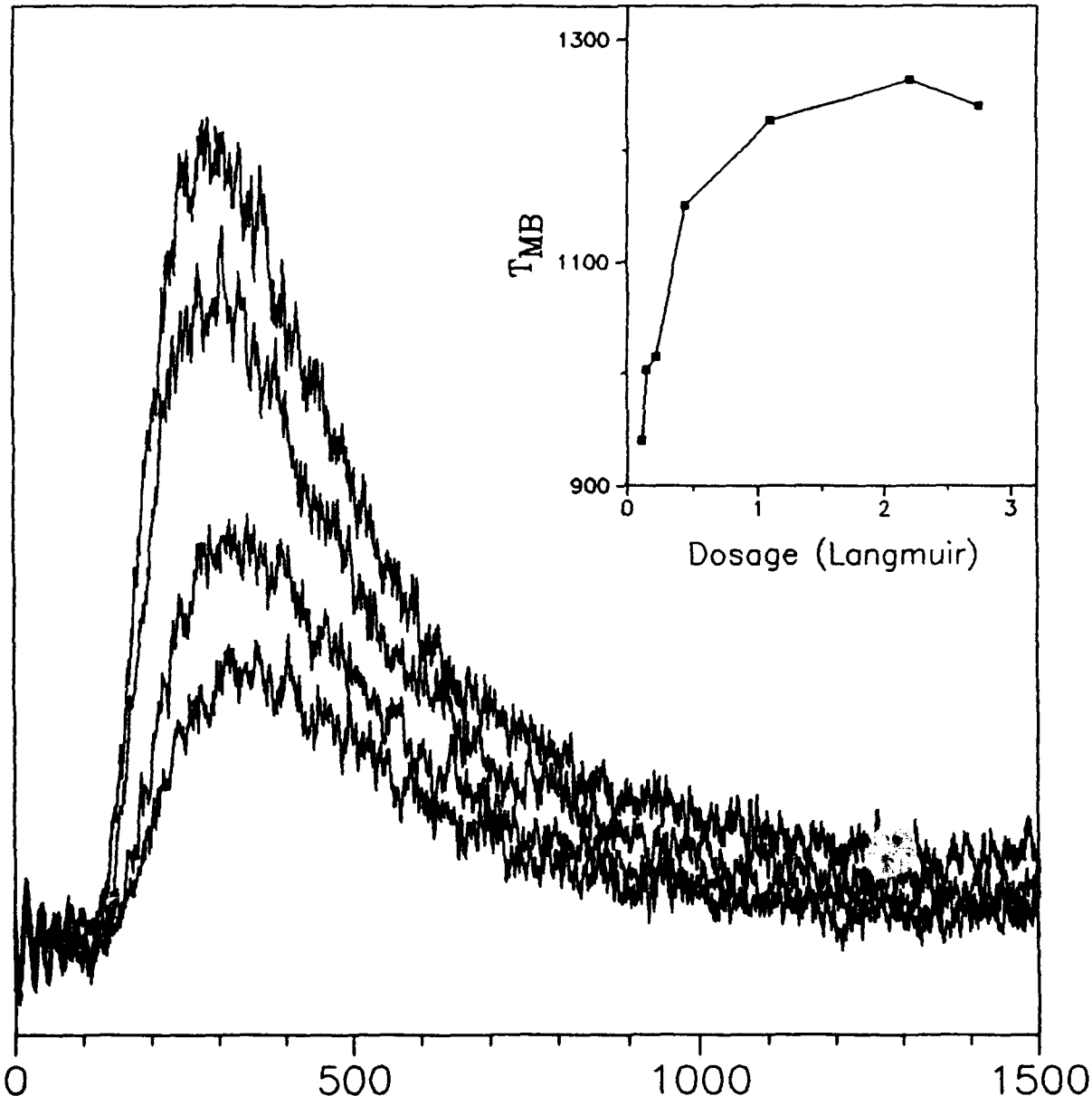
1300
1100
900
T_{MB}
0
1
2
3
Dosage (Langmuir)
0
500
1000
1500
Time of Flight (μsec)

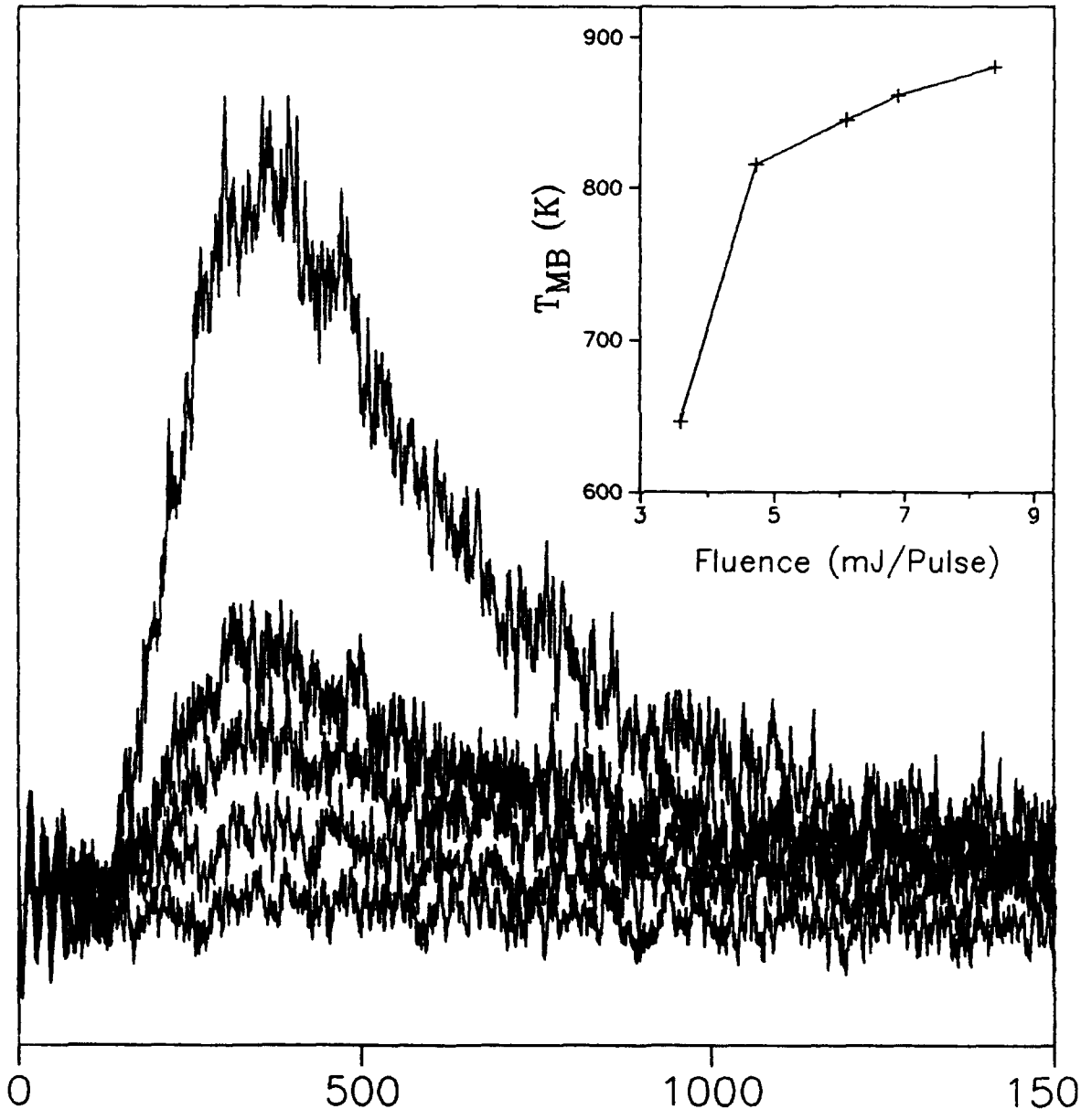
900
800
700
600
T_{MB} (K)
3
5
7
9
Fluence (mJ/Pulse)
0
500
1000
1500
Time of Flight (μSec)

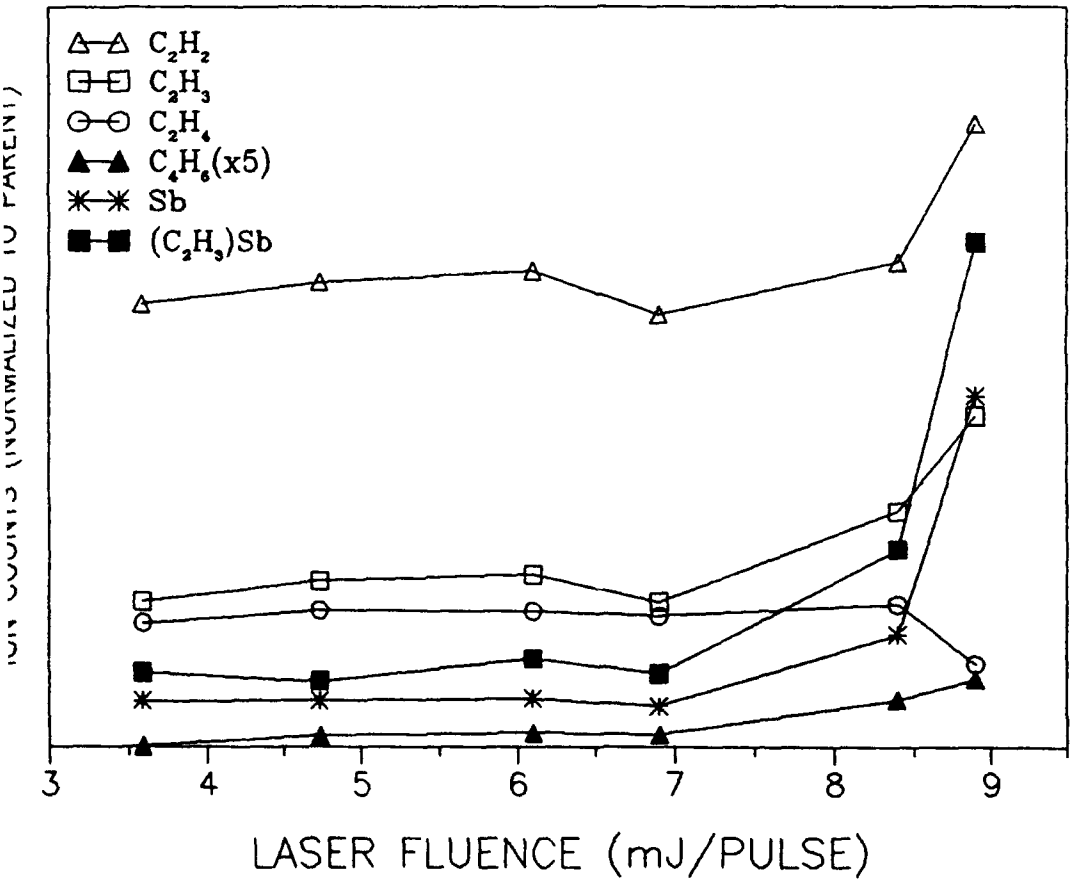
C_2H_2
C_2H_3
C_2H_4
C_4H_6(x5)
Sb
$(C_2H_3)Sb$
3
4
5
6
7
8
9
LASER FLUENCE (mJ/PULSE)

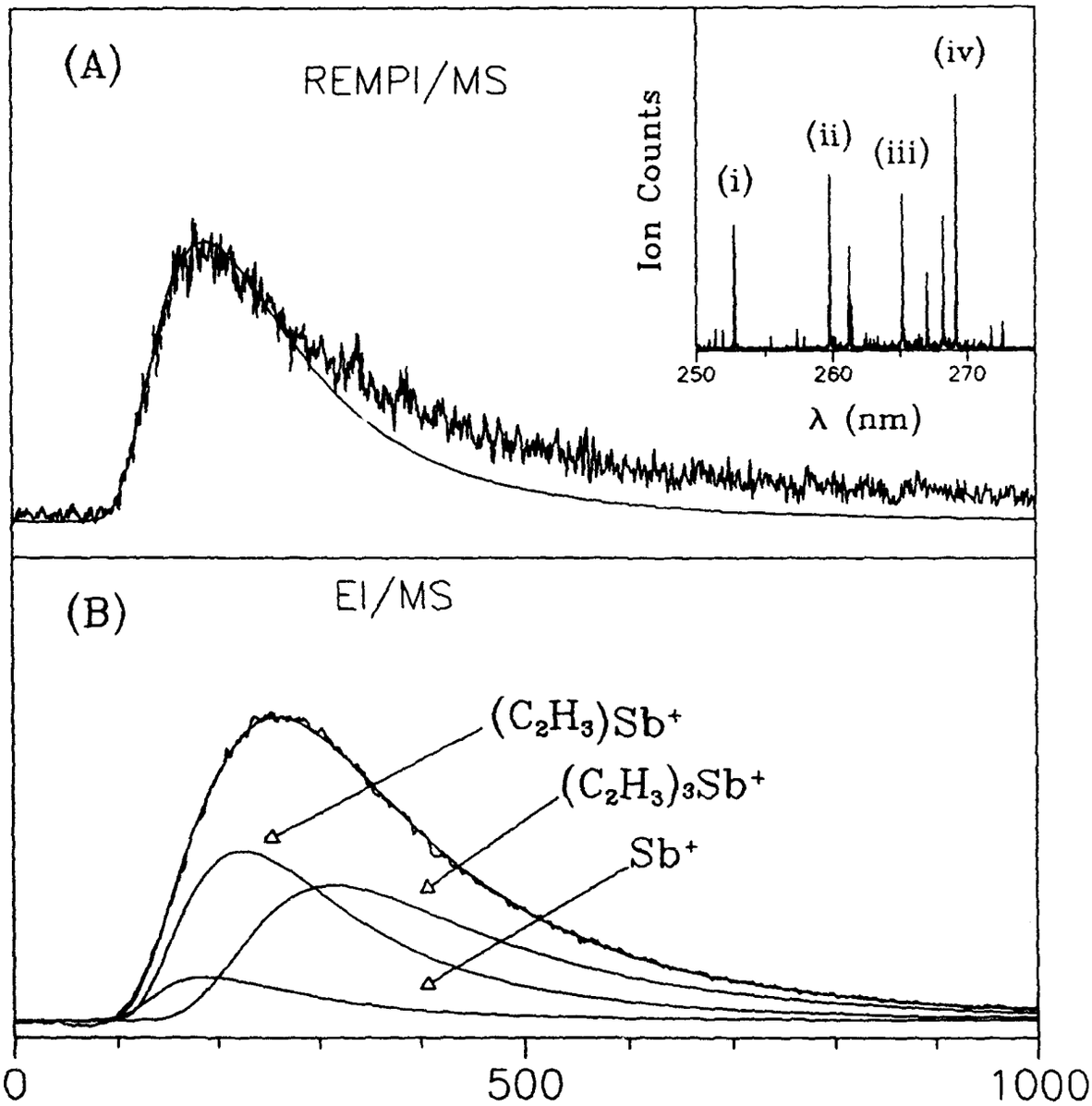
(A)
REMPI/MS
Ion Counts
(i)
(ii)
(iii)
(iv)
250
260
270
λ (nm)
(B)
EI/MS
$(C_2H_3)Sb^+$
$(C_2H_3)_3Sb^+$
Sb^+
0
500
1000
Time of Flight (μsec)